Available online at www.CivileJournal.org

Civil Engineering Journal

(E-ISSN: 2476-3055; ISSN: 2676-6957)

Vol. 12, No. 01, January, 2026

High-Resolution Silt Distribution Mapping Using Ordinary Kriging From Borehole Data in a Geohazard-Prone Area

Mohammad Radzif Taharin [1*], Nazaruddin Abdul Taha [1], Adriana Amaludin [1], Mohd Shaifuddin Abdul Razak [2], Muhammad Farid Zulkifli [3], Chow Wai Ming [3]

[1] *Intelligent Construction Research Group, Faculty of Engineering, Universiti Malaysia Sabah, 88450 Kota Kinabalu, Sabah, Malaysia.*

[2] *Slope Engineering Department, Jabatan Kerja Raya Malaysia, Kuala Lumpur, Malaysia.*

[3] *Jurutera Inovasi Sdn. Bhd., Kota Kinabalu, Sabah, Malaysia.*

Received 01 September 2025; Revised 21 December 2025; Accepted 27 December 2025; Published 01 January 2026

Abstract

Kundasang, Sabah, is one of the most geohazard-prone highland regions in Malaysia. Slope failures are frequently triggered by heavy rain. Silt-rich zones present a particular stability problem, since silt has low cohesion and drains faster than clay, which means that slopes can undergo rapid saturation and lose shear strength during sustained and intense rainfall. Previous research works in Kundasang have focused on landslide susceptibility through rainfall thresholds and GIS terrain analysis. However, depth-specific, high-resolution silt distribution maps have not yet been produced. This study addresses the research gap using geostatistical modeling of geotechnical data from boreholes to map silt distribution patterns. Soil samples from 70 boreholes were analyzed by classifying soil types down to 10 m depth in 2.5 m segments. Using Ordinary Kriging in ArcGIS 10.3, the best-fit semivariogram model for each depth was selected based on the lowest Root Mean Square Error values (ranging from 5.33 to 11.92). The findings reveal that high-silt zones (areas with over 30% silt content) cover around 40% of the study area and cluster mainly in western and northern Kundasang, particularly in the upper 7.5 m of soil. These correspond to areas previously documented as highly susceptible to rainfall-induced slope failures. The depth-specific silt distribution maps produced in this study provide important geotechnical inputs to enhance future landslide susceptibility assessments, improve slope stability analyses, and support risk-informed land-use planning for local authorities in geohazard-prone highland areas.

Keywords: Ordinary Kriging; Geostatistical Modeling; Silt Distribution Mapping; Semivariogram; Borehole Data.

1. Introduction

In tropical and mountainous regions, steep terrain and heterogeneous soil compositions are inherent factors that cause slope instability. These conditions are further aggravated by prolonged or intense rainfall, ultimately inducing major geohazards in the form of rainfall-induced slope failures. Within the heterogeneous soil components, silt-rich zones, often found near hilly areas [1, 2], are particularly important to identify for slope stability assessments. Although silt is favorable for agricultural productivity due to its high nutrient retention and water-holding capacity [3, 4], it possesses low cohesion and moderate permeability (higher than clay but lower than sand), making it susceptible to rapid saturation, pore pressure build-up, and shear strength loss during prolonged rainfall events [5, 6]. The combination of steep terrain and rapid saturation of silt-rich zones contributes to soil movement in hilly areas, triggering shallow translational slides and debris flows [7].

* Corresponding author: radzif@ums.edu.my

https://doi.org/10.28991/CEJ-2026-012-01-017

Kundasang, located on the southwestern base of Mount Kinabalu, is considered one of the most geohazard-prone highland areas in Malaysia, despite being one of the top tourist destinations in the state of Sabah due to its proximity to the country's highest mountain. Despite its importance as a tourism and agricultural hub, Kundasang is highly susceptible to rainfall-induced soil movements, landslides, and debris flows, which have severely impacted public infrastructure, farmlands, and residential areas [8, 9]. As noted earlier, identifying silt-rich zones within the Kundasang area is imperative, as these zones significantly increase the risk of slope failures, posing threats to local residents and potential damage to property and infrastructure.

Previous landslide susceptibility studies in Kundasang have primarily employed GIS-based terrain analysis and statistical methods. Roslee et al. [10] produced landslide susceptibility maps using factor analysis models, while Shahrir et al. [11] applied bivariate frequency ratio approaches to assess natural and artificial slopes. More recently, Krishnan et al. [12] developed a debris-flow susceptibility map from Pekan Nabalu to Kundasang using weights-of-evidence modeling, and Roslee et al. [8] applied frequency ratio models to produce a debris-flow susceptibility map for the area. In addition, Mohd Salleh et al. [13] utilized vegetation anomaly indicators derived from remote sensing to classify translational landslide activity. Although these studies successfully identified high-risk zones using topographic, hydrological, and environmental factors, they did not characterize the depth-specific subsurface geotechnical variability that strongly influences slope stability.

Despite advances in surface-based susceptibility modeling, a critical research gap remains in understanding the three-dimensional subsurface distribution of problematic soil layers, particularly silt-rich zones known to be highly susceptible to rainfall-induced failures. Previous studies in Kundasang relied on generalized geological maps without systematic spatial interpolation to produce continuous, depth-specific geotechnical profiles. This limitation is significant because slope stability depends not only on surface terrain but also on variations in soil properties with depth. The shallow subsurface (0–10 m) is especially important, as high silt content at these depths is problematic, given that most landslides in Kundasang fail along planes within this zone.

Recent advances in geostatistical modeling now enable the production of high-resolution subsurface soil maps that illustrate both vertical and spatial variability in soil properties. To address this gap, the present study employs geostatistical modeling—specifically Ordinary Kriging (OK)—to map the spatial and vertical variability of silt using systematic borehole data. Unlike previous GIS-based susceptibility models that rely on surface terrain attributes, OK provides a framework for interpolating subsurface geotechnical properties while accounting for spatial autocorrelation and quantifying prediction uncertainty through semivariogram analysis. In this study, the OK method was applied to generate high-resolution, depth-specific silt distribution maps for Kundasang town, capturing the three-dimensional heterogeneity of subsurface conditions. To the best of the authors' knowledge, this is the first subsurface characterization study in Sabah using geostatistical methods. Two primary objectives were established: (i) to determine the optimal semivariogram models for accurate spatial prediction of silt content using Root Mean Square Error (RMSE)-based evaluation, and (ii) to produce layered silt distribution maps at 2.5 m intervals from 0 to 10 m depth. The outputs provide essential geotechnical inputs for comprehensive landslide susceptibility assessment, slope stability analysis, and risk-informed land-use planning in geohazard-prone highland areas such as Kundasang.

The remainder of this paper is organized as follows: Section 2 describes the study area, including its geological characteristics and documented geohazard events. Section 3 presents the geotechnical data sources and explains the selected geostatistical methodology, including the Ordinary Kriging method and semivariogram model selection. Section 4 presents the results and discussion, analyzing semivariogram performance and depth-specific silt distribution maps and relating these findings to documented slope failures. Section 5 provides the study's conclusions and recommendations for future research.

2. Study Area

2.1. Location and Geological Characteristics

Kundasang town (Figure 1-a) is located on the terrain formed by the Trusmadi and Crocker Formations [10, 14]. Figure 1-b shows that the area has steep slopes, with some places exceeding 35° [15]. Table 1 summarizes the main soil units, landform features, and typical properties of each formation. The geological map (Figure 2) produced by Roslee et al. [14] shows that Kundasang is mostly on the Trusmadi Formation [16]. While the geological map gives a broad picture of subsurface conditions affecting slope behavior, the borehole data presented in this study provides much finer detail on the geotechnical properties across the study area.

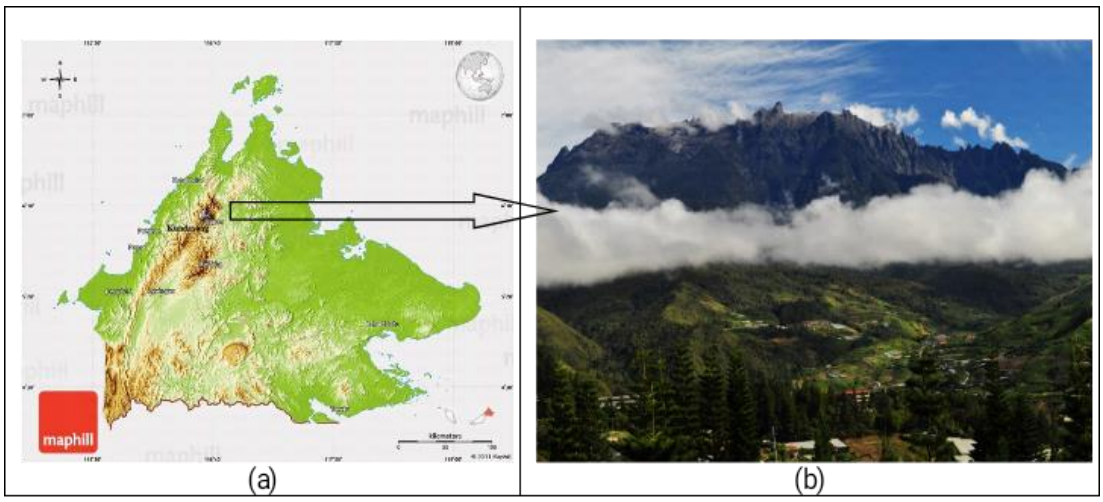

Figure 1. (a) Location of Kundasang, Sabah. (b) View of Mount Kinabalu and Kundasang town

Table 1. Formation and Soil Properties in Kundasang, Sabah

Formation Properties	Trusmadi Formation	Crocker Formation
Lithology	Phyllite and slate	Interbedded sandstone-shale and shale
Landform	Mountains above 1200 m (4000 ft) above sea level	Mountains
Main Soil Units	Greyic and Orthic Acrisols, Gleyic Podzol, Humic Gleysols, Dystic Histosol, and Lithosol	Orthic Acrisol, Chromic and Dystric Cambisols, and Lithosol
Weathering Grade	IV to VI	IV to VI
Cohesion, c (kPa)	5.11 – 15.34	3.2 – 17.27
Angle of Internal Friction (^{0})	7.72^0 - 26.65^0	7.70^0 - 29.50^0
Plasticity Index (PI)	14 – 23	12 – 23
Sand percentage (%)	22 – 42	22 – 70
Silt Percentage (%)	18 – 57	7 – 57
Clay Percentage (%)	22 – 43	15 – 45
Moisture Content (%)	5 – 25	5 – 35

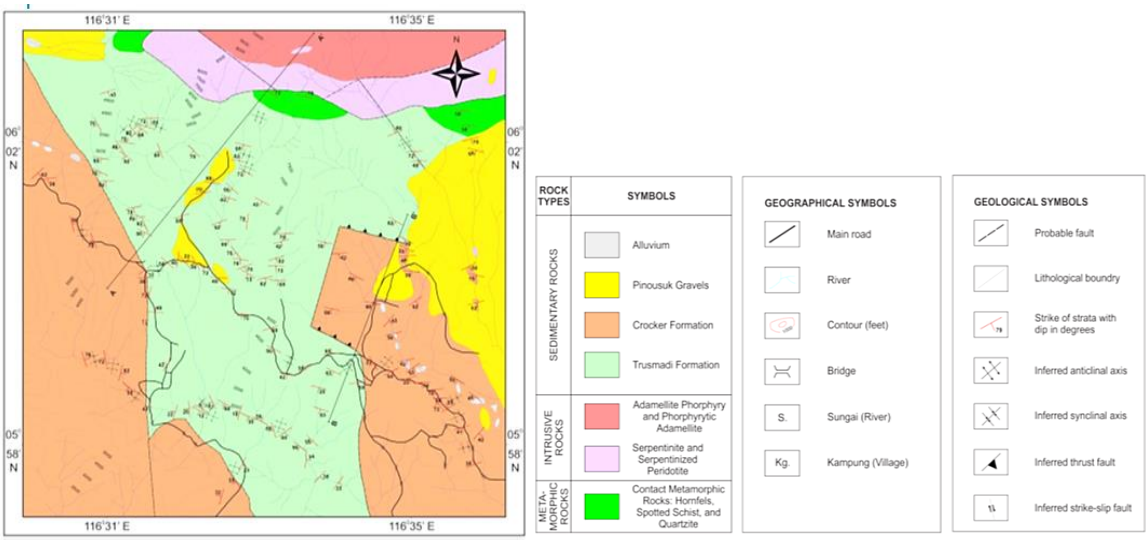

Figure 2. Geological map of Kundasang, Sabah [14]

The different rock types in these formations directly influence the slope behavior and failure. In the humid tropical climate of Kundasang, the phyllite and slate of the Trusmadi Formation are subjected to chemical weathering [14], breaking down the parent material into clay- and silt-rich residual soil. These fine-grained soils have low cohesion (see Section 4.1) and moderate permeability, making it vulnerable to pore pressure buildup during sustained rainfall. Once saturated, effective stress drops and shear strength deteriorates [6], leading to shallow translational slides at depths of 2.5 – 7.5 m where silt concentration is at its highest [14, 17]. In contrast, the Crocker Formation is the complete opposite,

where its sandstone breaks down into coarser material with better drainage and higher angle of friction, therefore resulting in fewer rainfall-triggered shallow failures. However, deep-seated failures and structurally controlled instabilities still occur due to weak bedding planes and toe erosion [11]. The clustering of slope failures in the Trusmadi Formation is attributed to these factors, and the failure locations align with the high-silt zone maps in Section 4.3.

2.2. Documented Geohazard Occurrences

Kundasang ranks among Malaysia's more landslide-prone highland regions due to its steep terrain, weathered bedrock, and heavy rainfall. In Kundasang, rainfall-related landslides and debris flows are a recurring concern, creating challenges for infrastructure, farmlands, and tourism facilities [8, 9, 18]. A well-known case study is the gradual ground movement at SMK Kundasang, where ongoing soil displacement caused extensive damage to the school buildings and surrounding infrastructure, that authorities relocated the school in 2012 [15]. Inclinometer measurements in Figure 3 show subsurface displacement near the school, and Figure 4 shows ground deformation on the school grounds (IKRAM, 2000). Regional landslide hazard assessments have identified Kundasang as a highly susceptible area, a classification supported by previously recorded events [10, 11].

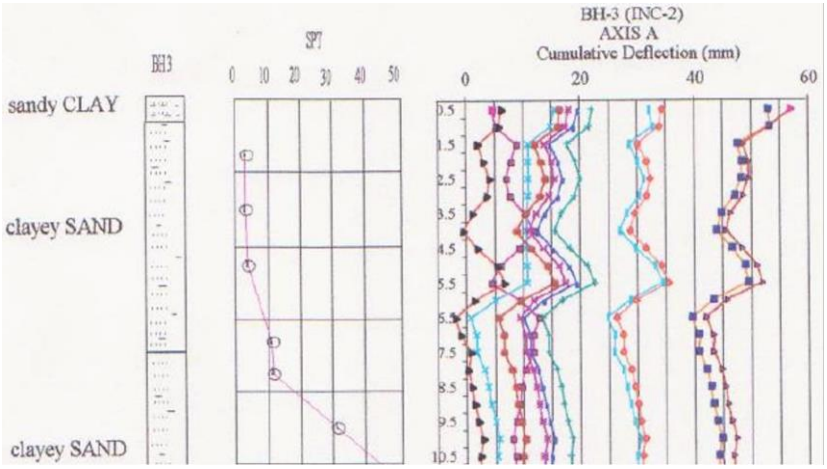

Figure 3. Inclinometer readings indicating subsurface ground movement between 2.5 m and 6.5 m depth [19]

Figure 4. Ground deformation at SMK Kundasang caused by progressive soil movement [19]

Surface-based landslide susceptibility maps have been created for Kundasang (e.g., Krishnan et al. [12]), but only a few researchers have examined how geotechnical properties change with depth and affect slope stability. Filling this research gap is important, since depth-specific geotechnical data would strengthen hazard forecasting and enable more informed land-use decisions in Kundasang through engineering analyses.

3. Geotechnical Data and Geostatistical Method

3.1. Borehole Dataset

For this study, data from 70 boreholes distributed across Kundasang town were utilized to extract subsurface geotechnical information (Figure 5). These records allowed the geotechnical characterization of the study area, to help understand the soil properties that influenced their engineering behavior. The dataset was originally compiled for the purpose of design and construction of retaining walls and other infrastructure works carried out in response to active soil movements recorded between 2000 and 2001 [17, 20]. Shear strength parameters (cohesion, angle of friction)

reported in Section 4.1 (Soil Classification) were obtained from consolidated isotropic undrained (CIU) triaxial tests conducted on the soil samples, which provide effective stress values by taking into account the pore water pressures during the shearing stage.

Figure 5. Borehole locations of study area in Kundasang, Ranau, Sabah

This analysis focuses on the upper 10 m of the soil, divided into four 2.5 m layers to examine the change of silt content with depth. A geostatistical method, Ordinary Kriging (OK), as presented in Section 3.2, was used to map silt variability. The 10 m borehole depth was chosen to capture the critical failure zone for translational slides in Kundasang. Inclinometer monitoring (Figure 3) shows that the subsurface ground movement happens between 2.5–6.5 m, with measurements extending to 10.5 m where conditions remain stable below the active shear zone [19]. Post-failure investigations and remedial work recorded by JKR [17, 20] confirm that most shallow translational failures in Kundasang occur at similar depths. The 0–10 m investigation depth therefore captures the zone where most translational slides occur, as validated by the measured ground movements and documented slope instability events. Additionally, this depth range represents the extent of available historical data with consistent soil characterization across all 70 locations, which allows thorough geostatistical analysis at four 2.5 m intervals to be carried out accordingly. The inclusion of the 7.5–10 m interval, despite being below the typical failure zone (2.5–7.5 m as documented in Section 2.1), serves two purposes: (1) it provides a control depth to demonstrate the methodology's ability to detect the absence of spatial structure in geotechnically stable zones (as seen by the flat semivariogram at this depth, explained in Section 4.2), and (2) it ensures complete characterization of the full investigation depth used in the original geotechnical studies.

The 70 boreholes were derived from several geotechnical site investigation reports conducted between 2000 and 2001, mostly along road corridors and development sites (Figure 5). These investigations targeted locations where slope failures had already occurred, rather than following a systematic grid pattern. When the borehole locations (Figure 5) were overlaid on the geological map (Figure 2), an uneven distribution of the borehole was obvious. About 48–50 boreholes (~70%) are in the Trusmadi Formation (in western and northern sectors), while 20–22 boreholes (~30%) are in the Crocker Formation to the east. This imbalance reflects where the geotechnical work is mostly concentrated: on higher-risk areas within the Trusmadi Formation, where phyllite and slate weather into silt-rich soils that are vulnerable to rainfall-induced failure. Despite the unbalanced sampling between formations, the borehole distribution shows variable spacing patterns across the study area (Figure 5). Dense sampling with approximately 100–300 m spacing was obtained in the western and central sectors, while sparser coverage (400–800 m spacing) characterizes the eastern Crocker Formation sector. This sampling pattern is considered sufficient for exploratory geostatistical characterization at the regional scale, though the authors acknowledge that the prediction uncertainty is higher in the under-sampled zones. Future site-specific assessments in the eastern sector should include systematic investigation grids at 200–300 m spacing to reduce kriging variance and improve prediction reliability for site-level engineering design.

The silt percentage data wasn't adjusted for elevation or slope angle. The raw particle size test results were used for the spatial interpolation to preserve natural soil variability across the site. OK accounts for spatial trends through semivariogram modeling without requiring elevation normalization. Topographic position and slope angle affect weathering and soil development, but these influences show up in the measured silt content values and get built into the interpolated surfaces automatically.

3.2. Ordinary Kriging and Semivariogram Models

Ordinary Kriging (OK) was chosen as our geostatistical method because of its effectiveness for modeling spatial variability in geotechnical data. D.G. Krige developed the technique in the 1950s for estimating mineral resources, and

Georges Matheron expanded and formalized it in the 1960s. OK has since become fundamental to geostatistics in earth and environmental sciences [21-24]. Seven decades after Krige and Matheron's foundational work, recent works show that OK remains reliable for creating high-resolution geotechnical and environmental maps in complex terrain [25-28].

The OK method was applied to interpolate silt content variability across Kundasang. The advantage of OK is its ability to model spatial correlation between borehole sampling points and estimate values where samples were not available [29, 30], which is useful in heterogenous terrain like Kundasang [14]. Unlike deterministic interpolation methods such as Inverse Distance Weighting (IDW), OK not only predicts unknown values, but also estimates prediction error, which produces higher quality subsurface variability maps [31, 32].

OK models spatial autocorrelation explicitly through the semivariogram to achieve Best Linear Unbiased Prediction (BLUP), whereas deterministic methods simply apply arbitrary distance-weighting formulas [22, 33]. Three factors make OK valuable for subsurface soil characterization. Soil properties show scale-dependent spatial patterns that reflect depositional and weathering history, which need to be measured from the data. Next, OK calculates prediction variance (kriging variance) at every location, which allows spatial uncertainty to be quantified for risk-informed slope stability decisions. Lastly, OK predictions match actual borehole measurements at sample locations and have realistic transitions in soil properties between boreholes [31]. These characteristics make OK suitable for mapping subsurface geotechnical heterogeneity in geohazard-prone areas where prediction reliability must be quantified.

The predicted value, *Z(s)* at an unsampled location *s*, can be expressed as:

$$Z(s) = \mu + \varepsilon(s) \quad (1)$$

where μ is an unknown constant mean of the regionalized variable across the study area, and $\varepsilon(s)$ is random error term representing local spatial variability (assumed to have zero mean, spatially uncorrelated).

From Equation 1, the population mean is assumed to be as a true but unknown constant, estimated from the overall trend of the observed data [33, 34]. This concept is illustrated in Figure 6, which shows the example of an OK prediction surface generated using the Geostatistical Analyst extension in ArcGIS 10.3. To determine spatial characteristics, four theoretical semivariogram models, namely the Spherical, Exponential, Circular and Gaussian models were evaluated (Figure 7) [35, 36].

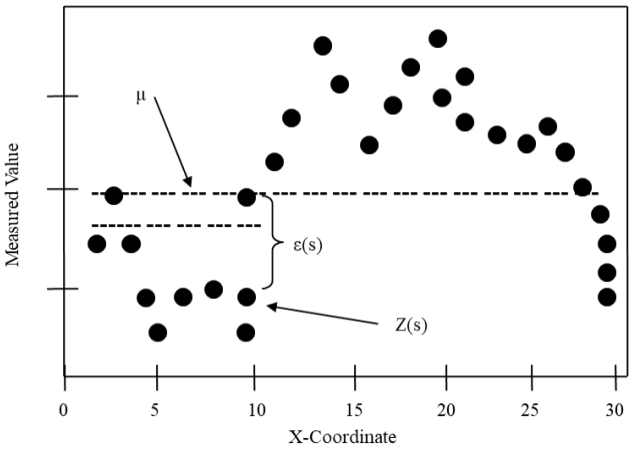

Figure 6. Example of an Ordinary Kriging (OK) prediction surface generated using ArcGIS 10.3 [35]

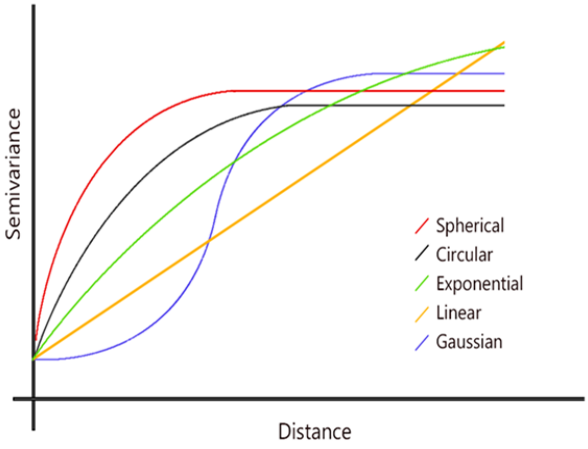

Figure 7. Candidate semivariogram models used for Ordinary Kriging prediction with ArcGIS 10.3 [35]

Each model was fitted to the experimental semivariogram of silt content, and the optimal model for each depth interval was selected based on the lowest Root Mean Square Error (RMSE). These semivariograms were then applied in the OK interpolation to generate depth-specific silt distribution maps. Isotropic semivariogram models were used for this analysis, assuming uniform spatial correlation in all directions. While directional variability (anisotropy) was not formally tested, this assumption is considered reasonable given: (1) the irregular topography and complex geological structure of Kundasang, which would make directional trends difficult to model with the existing borehole spacing; Isotropic semivariogram models were used for this analysis, assuming uniform spatial correlation in all directions. While directional variability (anisotropy) was not formally tested, we acknowledge this as a methodological limitation.

The visible NNE-SSW trending geological contact between Trusmadi and Crocker Formations (Figure 2) suggests potential structural anisotropy may exist. However, formal anisotropy assessment was not conducted due to: (1) the existing borehole distribution lacking systematic directional sampling required for robust directional semivariogram estimation (minimum 30–50 data pairs per direction bin recommended) [37], (2) computational constraints of the standard ArcGIS Geostatistical Analyst toolset used in this study, and (3) the current study being an exploratory regional-scale characterization establishing baseline methodology. As such, future studies with systematically designed sampling grids oriented relative to geological structures should investigate potential anisotropic effects to improve prediction accuracy in structurally complex terrain.

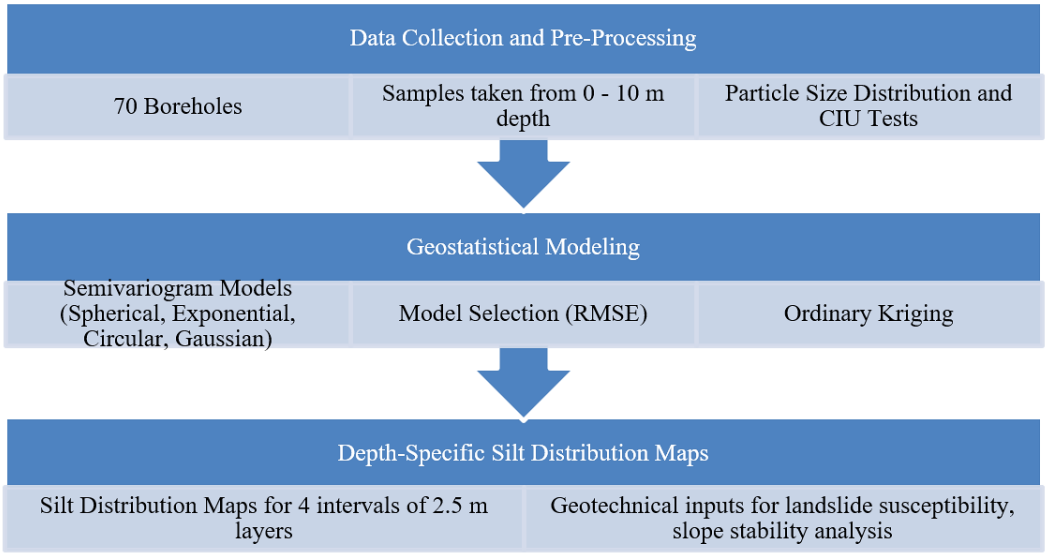

Figure 8. Research methodology flowchart

As mentioned previously, there were no data transformations that were applied to the silt data prior to geostatistical analysis. Silt percentage data typically shows relatively symmetric distributions within the natural range of soil compositions, especially when compared to highly skewed variables such as contaminant concentrations or mineral grades. Even though formal normality testing (for instance, the Shapiro-Wilk test) was not conducted, the assumption of approximate normality of the OK method is considered adequate for this study. Furthermore, the RMSE-based model selection procedure used in this study selects models that produce accurate predictions (regardless of the data distribution), preventing any issues regarding data distribution. The outputs of the geotechnical and geostatistical analyses are presented in the Results section, starting with soil characterization (Section 4.1), followed by the semivariogram evaluation (Section 4.2) and the depth-specific silt mapping results (Section 4.3). Figure 8 shows the research methodology flowchart showing the workflow from data collection to the silt distribution mapping.

4. Results and Discussion

4.1. Soil Characterization

Characterization of the subsurface soils is important because their physical and mechanical properties directly control slope stability in Kundasang. Knowing the relative proportions of sand, silt, and clay, along with shear strength parameters from borehole data, gives the context to interpret the silt content maps and understand what they mean for slope stability.

Figure 9 shows how sand, silt, and clay are distributed across the borehole samples, broken into four depth intervals down to 10 m. Gravel was not included because reporting was inconsistent across boreholes, and it makes up only a small fraction compared to sand, silt, and clay. After removing gravel, the remaining soil fractions were normalized so that they total 100% at each depth.

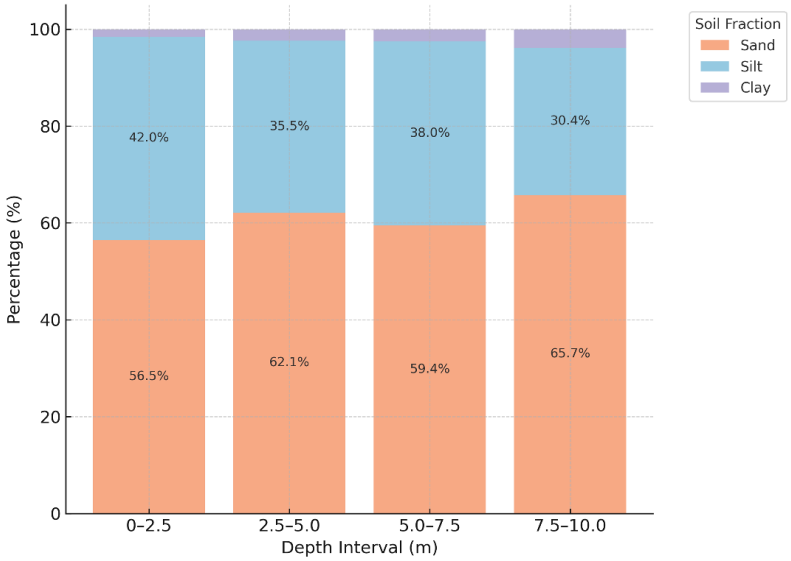

Figure 9. Normalized sand, silt and clay distribution across four depth intervals in Kundasang borehole dataset

Figure 9 makes clear that sand and silt dominate the soil at all depths, with clay playing a minor role. In these sand-silt mixtures, silt contributes to lower cohesion and higher permeability than clay would, while sand provides the friction angle. When rainfall continues for hours or days, water infiltrates these sand-silt soils and saturates the silt particles, triggering shear strength loss from excess pore pressure that eventually causes rainfall-induced slope failures [7, 38].

Table 2 lists key geotechnical parameters from consolidated isotropically undrained (CIU) triaxial tests: cohesion (c), friction angle (ϕ), and Atterberg Limits. Cohesion values are low, ranging from 0 to 13 kPa, which classifies these as "very soft" soils under BS 5930 [39]. Friction angles fall between 21° and 35°, consistent with the high granular content. Liquid Limits vary from 23 to 51% while Plasticity Index values range 10% to 29%. Both indicate low to intermediate plasticity. These low cohesion values paired with moderate friction angles reflect the soil distribution trend shown in Figure 9, sand and silt consist most of the soil. This type of soil composition is prone to strength loss under saturation [40, 41], in line with documented reports of rainfall-induced slope failures in Kundasang [13, 42].

Table 2. Descriptive statistics of shear strength parameters and Atterberg Limits and borehole soils in Kundasang

Range	Cohesion, c [kPa]	Angle of Internal Friction, ϕ [^{0}]	Liquid Limit [%]	Plasticity Index [%]
Minimum	0	21.61	23	10
Median	5.08	29.46	33	17
Maximum	13.19	35.31	51	29
Mean	5.53	29.41	34.25	17.60

Therefore, the Kundasang subsurface soil is dominated by sand–silt matrices with low to intermediate plasticity clays, due to a heterogeneous soil profile derived from the Trusmadi and Crocker formations. The soil distribution shown in Figure 9, and shear strength parameters presented in Table 2 highlights the importance of mapping silt variability. In particular, silt-rich zones are vulnerable to rainfall-induced shear strength loss which ultimately leads to slope failures. The findings in this section provide a comprehensive basis for the semivariogram modeling, and depth-specific silt distribution mapping presented in the following sections.

4.2. Semivariogram Selection and Performance

This section evaluates the performance of candidate semivariogram models to identify the most optimal model for Ordinary Kriging (OK) interpolation at each depth interval. The selection of a suitable semivariogram model is critical, as it influences the accuracy of the OK predictions. The most suitable model minimizes estimation errors and therefore improves the reliability of the interpolated maps [31].

Table 3 presents the RMSE values obtained from the fitted semivariogram models across the four depth intervals. No single model was consistently optimal across all depths, illustrating the heterogeneity of the subsurface conditions. The fitted semivariograms represent the spatial structure of the accumulated borehole data, representing the "data cloud" from which the optimal model for each depth was selected. In doing so, this allows the zones with higher silt content relative to the surrounding areas to be emphasized. This highlights areas where silt concentrations exceed neighboring zones. The fitted semivariogram models for 0 to 10 m depth appear in Figure 10.

Table 3. RMSE values for the tested semivariogram models across four depth intervals

Semivariogram Model	0 – 2.5 [m]	2.5 – 5.0 [m]	5.0 – 7.5 [m]	7.5 – 10 [m]
Spherical	8.8624	10.3022	5.7722	11.9208
Exponential	8.5935	10.3318	5.8788	11.9208
Circular	8.6688	10.2856	5.7309	11.9208
Gaussian	9.6413	10.3450	5.3323	11.9208

Figure 10 does not show one model dominating the entire soil profile. The pattern actually shifts with depth. In the uppermost layer (0–2.5 m), the exponential model produced the lowest RMSE, which is not surprising because near-surface soils usually change gradually rather than abruptly. Once we go slightly deeper, roughly 2.5–5.0 m, the circular model begins to fit better. The behavior there shows a steady rise in silt percentage at short to medium distances. At 5.0–7.5 m, the Gaussian model gives the best fit, and its curve rises much more sharply at mid-range distances, which often points to pockets of material or clustered deposits [33]. Below 7.5 m, all the semivariogram models gave almost identical RMSE values. The curve is basically flat, meaning there is no strong spatial structure to capture at that depth [22, 43].

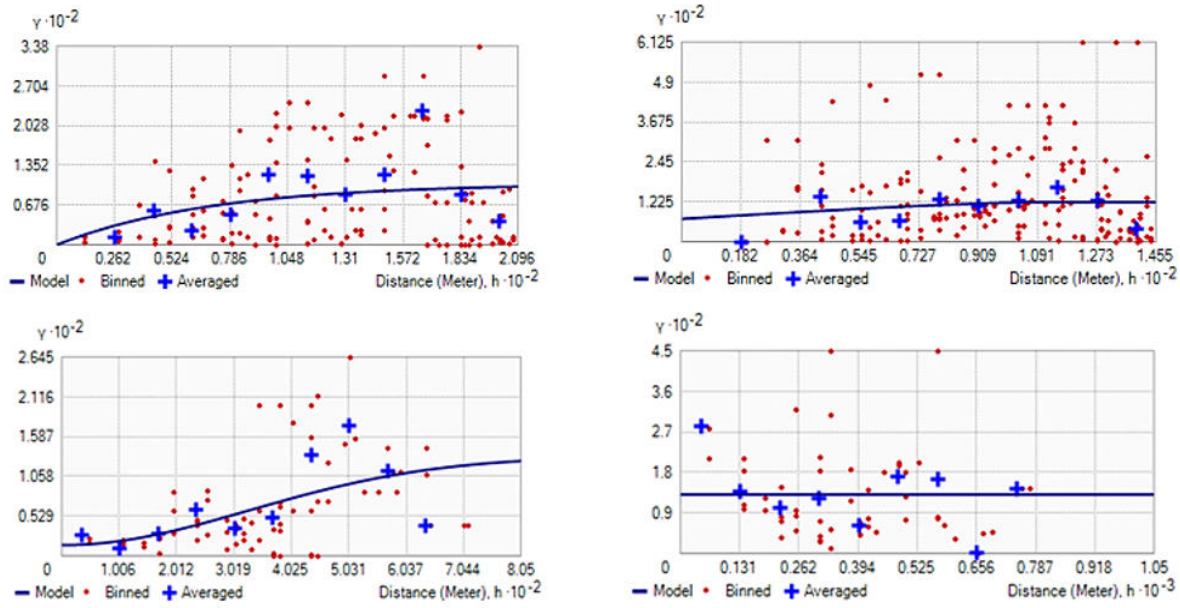

Figure 10. Fitted semivariogram models with the lowest RMSE values for each depth interval: exponential (0-2.5m), circular (2.5-5.0m), gaussian (5.0-7.5m), and flat (7.5-10m)

The exponential model near the surface (0–2.5 m) reflects the weathered topsoil, which tends to be fairly uniform. The circular model in the next interval suggests gradual layering from sediment deposition over time. The Gaussian model at 5.0–7.5 m hints at irregular changes, probably related to discontinuous weathering in the Trusmadi Formation. After 7.5 m, the flat pattern could mean two things: either the boreholes are spaced too far apart to pick up subtle variation, or the soil is becoming more uniform as it approaches the less-weathered bedrock. From an engineering point of view, this is useful because shallow slope failures, which normally occur above 7.5 m, can be mapped and modelled with much more confidence than deeper ones.

Using a separate semivariogram model for each depth was therefore justified. When these best-fit models were applied in ordinary kriging, the output was a series of depth-based maps rather than one generalized map. These maps make it easier to identify silt-rich and silt-poor areas, which is important when analyzing rainfall-triggered slope movements in Kundasang. Section 4.3 presents the detailed map results and the interpretation that follows.

4.3. Depth-Specific Silt Distribution Maps

The aim of this section is to present the depth-specific silt distribution maps generated using Ordinary Kriging interpolation, based on the optimal semivariogram models selected in the previous section. These maps show the vertical and lateral variability of silt content across the study area, which allows the identification of zones where high silt proportions are of a concern to the slope stability, especially under heavy rainfall conditions.

The generated depth-specific silt distribution maps (Figure 11-a to 11-d) indicate distinct vertical and lateral variability of the silt content within the 0–10 m soil profile. In general, the silt content ranged between 24–34%, with lower silt percentages (< 25%) accounting for 60% of the mapped area, and higher silt percentages (> 30%) are concentrated in the remaining 40%. The western and northern sectors show the largest clustering of high-silt zones, while the southern and central regions exhibit lower silt proportions. However, at the deepest interval (7.5–10 m), the semivariogram results produced a flat structure, which resulted in scattered and irregular silt distribution as seen in Figure 11-d, which demonstrates the absence of a clear spatial trend at this depth.

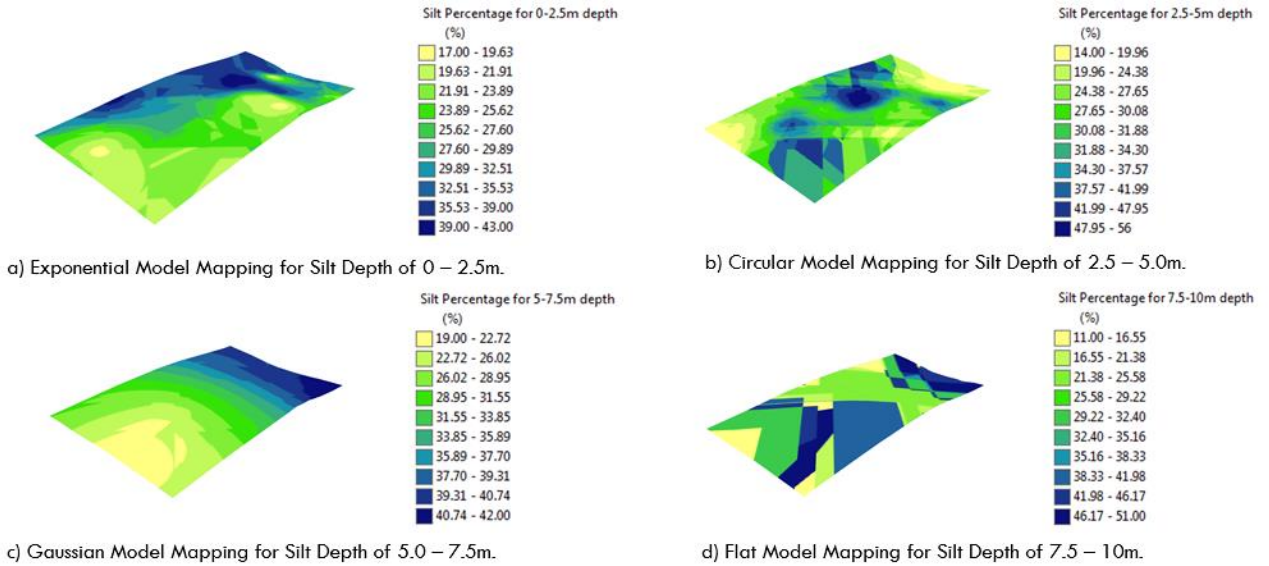

Figure 11. Depth-specific silt distribution maps generated using OK for four depth intervals

The concentration of high-silt zones in the western and northern sectors of Kundasang reflects the geological characteristics of the Trusmadi Formation, which consists of intensely weathered phyllite and slate that produce silt-sized particles through mechanical and chemical weathering. Conversely, lower silt content in the southern and central sectors correlates with the Crocker Formation, which largely consists of sandstone and shale that weather into coarser sand-dominated soils. These spatial patterns represent systematic outcomes of parent material weathering processes specific to each formation.

Therefore, these spatial patterns showcase the role of silt variability in predicting the slope response to rainfall events. Because silt-rich zones are typically attributed to higher permeability and lower cohesion compared to clay, the identified high-silt zones are more susceptible to rapid saturation, pore pressure build up and eventual loss of shear strength during intense or prolonged rainfall [5, 44]. This condition elevates the risk of rainfall-induced slope instability in these areas. In order to examine this relationship, the depth-specific silt distribution maps generated in this section are compared with the soil movement susceptibility map of Kundasang. The following section presents this comparison in detail, and evaluates the spatial correlation between high-silt zones and zones classified as highly susceptible to failure during intense rainfall events.

4.4. Relationship Between Silt Distribution and Soil Movement Maps

Comparing silt distribution with soil movement susceptibility is essential to evaluate the correlation between subsurface variability with slope instability under rainfall conditions. A comparison between the depth-specific silt distribution maps (Figure 11) and the soil movement susceptibility map shown in Figure 12 below exhibits a strong spatial association between silt-rich zones and areas classified as highly to very highly susceptible to soil movement. In most depth intervals, the zones with more than 30% silt fell within the areas classified as highly susceptible to soil movement. This pattern is visible throughout much of the profile. However, the 2.5 – 5.0 m interval does not follow it as closely, and the spatial match is weaker there. The situation changes again at 5.0 – 7.5 m. At this depth, pockets of high silt content overlap directly with the zones mapped as very highly susceptible, and this agreement appears consistently across the section. It is unlikely to be a random occurrence; rather, it indicates that variation in silt content exert a measurable control on slope response at depth.

Lower silt content does not guarantee stability. During intense rainfall, silt absorbs and holds water, which accelerates saturation. Once the soil reaches this state, shear strength can fall quite rapidly, and movement may initiate even without a high initial silt proportion [45]. Published works further supports this mechanism, with study results showing that slopes with minor gradients 5–10 subjected to rainfall with 60 mm/hr intensity are prone to detachment and transport [7, 46].

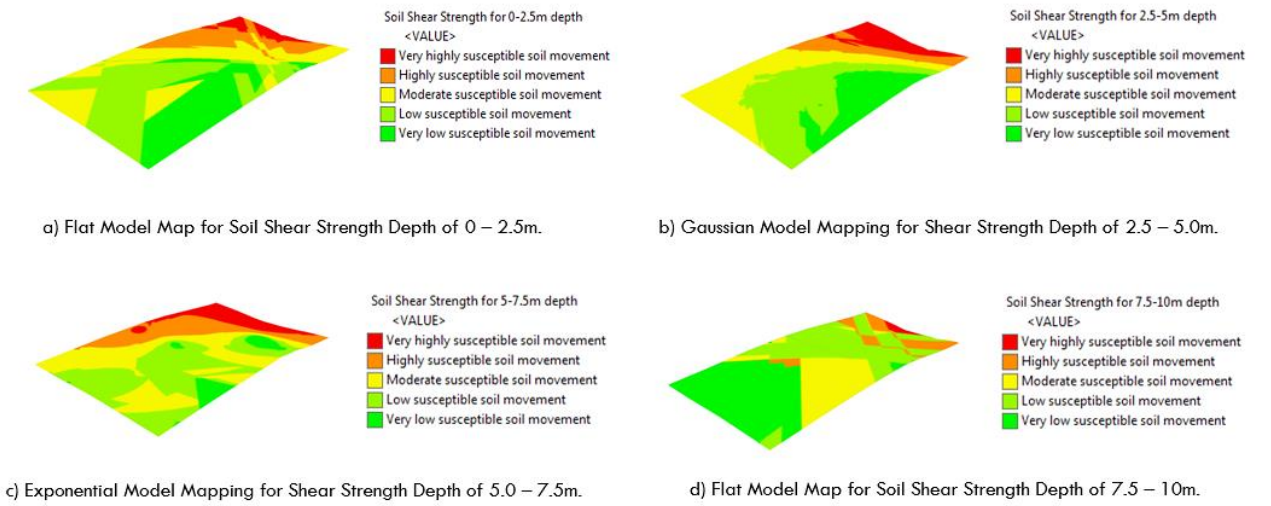

Figure 12. Soil movement susceptibility map of Kundasang showing zones from low to very high risk

The identification of silt-rich zones within an area highly prone to soil movement is therefore a key finding of this study. It provides an early indication of locations that are most at risk of rainfall-induced slope failures. Validation is provided by the documented progressive ground movements at SMK Kundasang (Figure 13), located in the northeastern part of the study area, where zones with high susceptibility to soil movement are directly correlated to the presence of low shear strength soil deposits [11, 12, 15].

As such, there is a strong agreement observed between the silt distribution maps, soil movement susceptibility map, with the recorded soil movement and slope failures in the study area. This highlights the reliability of the geostatistical analyses applied in this study, and therefore demonstrating the value of high-resolution, depth-specific silt mapping to improve the understanding of rainfall-driven landslide mechanisms. In addition, the silt maps also support proactive risk mitigation in the geohazard-prone highland environment such as Kundasang.

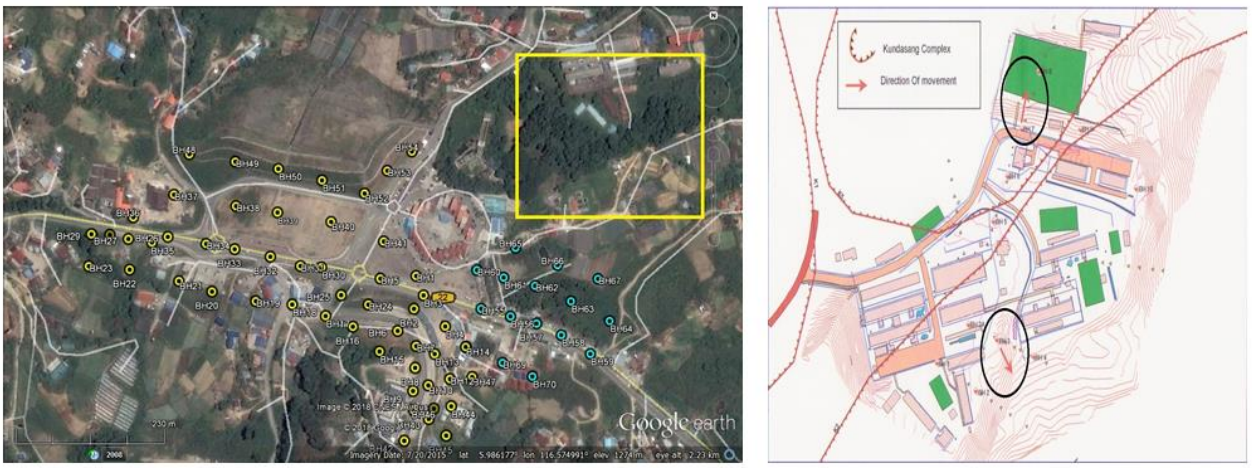

Figure 13. Soil movement affecting SMK Kundasang and the direction of progressive ground deformation

4.5. Comparison with Previous Landslide Susceptibility Studies

The silt patterns identified in this study generally match the geological interpretation of Roslee et al. [14]. The main difference is that the new maps incorporate depth information, so the changes in silt content with depth can be examined together with their lateral distribution across Kundasang. Surface geology does not show this behavior, because it only represents the formation boundaries. Roslee's work mapped the extent of the Trusmadi and Crocker Formations. After applying Ordinary Kriging to the borehole data, the subsurface results indicated that both formations contain internal variability. In other words, the formations do not behave as uniform units when examined below ground level. This contrast was visible because the interpolated maps produced a more detailed picture than surface mapping alone.

In the western and northern parts of the study area, where the Trusmadi Formation is more common, several locations recorded silt contents greater than 30 percent. Together, these pockets cover nearly 40 percent of that sector. They also coincide with areas mapped as Trusmadi phyllite and slate, suggesting that silt concentration is strongly influenced by local lithology. Field logging supported this interpretation, since highly weathered phyllite in several locations produced very fine material.

The results show that formation boundaries do not automatically represent uniform ground conditions. The seventy boreholes used in this study captured changes in silt content with depth, even within a single mapped unit. Two-dimensional maps cannot show this behavior. For slope assessment, this distinction matters: surface-based susceptibility models infer likely failure from terrain characteristics, but the subsurface mapping identifies weak, silt-rich layers directly. When both are considered together, hazard evaluations become more reliable, particularly in slopes where the underlying material controls how the ground behaves.

The predictive value of the silt distribution maps is supported by documented slope failures in Kundasang. Several historical geohazard events along the Tamparuli-Ranau route [17, 20] were accompanied by site investigations, and the post-failure observations reported silt-rich soils in the failed sections, which aligns with the interpolated results. Earlier studies were able to outline broad high-risk zones using statistical correlations between failures and terrain controls, but the current approach provides a direct geotechnical explanation. These slopes fail because they contain layers dominated by silt, which has low cohesion, moderate permeability and rapid loss of shear strength when subjected to heavy rainfall. With this information, mitigation becomes more targeted. Subsurface drainage, for instance, can be placed specifically within high-silt pockets where the loss of strength is most critical, resulting in more efficient and cost-effective slope protection strategies.

5. Conclusion

This work provides the first subsurface maps of silt distribution in Kundasang, Sabah with depth information resolved in 2.5 m intervals. Ordinary Kriging was applied to data from seventy boreholes, each logged to 10 m depth, in order to examine how silt content changes both vertically and across the landscape. Four semivariogram models were tested during the interpolation, and the optimal model for each depth layer was selected using RMSE values as the performance measure. The interpolated results show that several zones contain more than 30 percent silt, and these zones together cover roughly 40 percent of the study area. Many of these zones lie in the western and northern sectors, between 0 and 7.5 m depth, which matches the locations where slope failures have been reported. The agreement between the depth maps and the failure records, including the movement at SMK Kundasang, supports the interpretation that weak, fine-grained layers contribute to the instability of slopes in this region.

There are several practical implications. The maps help identify subsurface materials that may lose strength rapidly during intense rainfall, and this information is valuable for stability analysis where the likely failure plane lies within the upper 10 m of soil. The maps can also assist land-use planning by drawing attention to locations where mitigation or construction controls might be required. Some limitations should be acknowledged. The borehole data were collected from 2000 to 2001, and changes in land use or extreme rainfall could have altered subsurface conditions since that time. In the deepest interval, from 7.5 to 10 m, the semivariogram structure was almost flat, so additional sampling would be needed to confirm the behavior of that layer. Future research could incorporate rainfall thresholds, slope gradients, groundwater response and vegetation cover, so that a more comprehensive predictive model can be developed. When combined with real-time monitoring, such a model would improve early warnings for rainfall-triggered failures in Kundasang.

6. Declarations

6.1. Author Contributions

Conceptualization, M.R.T.; methodology, M.R.T.; software, M.R.T.; formal analysis, M.R.T.; investigation, M.R.T., A.A.; resources, M.R.T, M.S.A.R., M.F.Z., and C.W.M.; writing—original draft preparation, M.R.T.; writing—review and editing, M.R.T., N.A.T., and A.E.A.; funding acquisition, M.R.T, M.S.A.R., M.F.Z., and C.W.M. All authors have read and agreed to the published version of the manuscript.

6.2. Data Availability Statement

The data presented in this study are available in the article.

6.3. Funding and Acknowledgments

This research was supported by Universiti Malaysia Sabah (UMS) and Universiti Sains Malaysia (USM). Financial support provided by Jurutera Inovasi Sdn. Bhd. is gratefully acknowledged to facilitate the completion and publication of this work.

6.4. Conflicts of Interest

The authors declare no conflict of interest.

7. References

[1] Assallay, A. M., Rogers, C. D. F., Smalley, I. J., & Jefferson, I. F. (1998). Silt: 2-62 μm, 9-4φ. Earth Science Reviews, 45(1–2), 61–88. doi:10.1016/S0012-8252(98)00035-X.

[2] Bhavya, K., & Nagaraj, H. B. (2025). Influence of soil structure and clay mineralogy on Atterberg limits. Scientific Reports, 15(1), 15459. doi:10.1038/s41598-025-98729-y.

[3] Samuel, A., & Dines, L. (2022). Lockhart and Wiseman's Crop Husbandry Including Grassland. Woodhead Publishing, Sawston, United Kingdom. doi:10.1016/C2020-0-01095-9.

[4] Shahrokh, V., Bondi, G., Fahy, A., & O'Sullivan, L. (2025). Advancing Soil Compaction Assessment: A Comprehensive Study in Ireland. European Journal of Soil Science, 76(3), 70122. doi:10.1111/ejss.70122.

[5] Giannecchini, R., Zanon, A., & Barsanti, M. (2024). An Update on Rainfall Thresholds for Rainfall-Induced Landslides in the Southern Apuan Alps (Tuscany, Italy) Using Different Statistical Methods. Water (Switzerland), 16(5), 624. doi:10.3390/w16050624.

[6] He, X., Shi, W., Zhu, Y., Yan, L., Zhao, Y., & Wang, S. (2025). Coupled Effects of Fault-Related Groundwater Flow and Pore Water Pressure: Unraveling the Mechanisms of Deformation and Failure in Gentle Slopes. Arabian Journal for Science and Engineering, 50(18), 15015–15032. doi:10.1007/s13369-024-09925-3.

[7] Espinosa F, S. A., & El Naggar, M. H. (2024). Parametric Study of Rainfall-Induced Instability in Fine-Grained Sandy Soil. Geotechnics, 4(4), 1159–1174. doi:10.3390/geotechnics4040059.

[8] Roslee, R., Alexander, R. E., Sharir, K., Saidin, A., Warnana, D. D., Rochman, J. P. G. N., & Widodo, A. (2024). Mapping Debris Flow Susceptibility Using Frequency Ratio Model in Kundasang, Sabah, Malaysia. International Journal of Design & Nature and Ecodynamics, 19(5), 1581–1589. doi:10.18280/ijdne.190512.

[9] Rosli, M. I., Che Ros, F., Razak, K. A., Ambran, S., Kamaruddin, S. A., Anuar, A. N., Marto, A., Tobita, T., & Ono, Y. (2021). Modelling debris flow runout: A case study on the Mesilau Watershed, Kundasang, Sabah. Water (Switzerland), 13(19), 2667. doi:10.3390/w13192667.

[10] Roslee, R., Jamaluddin, T. A., & Talip, M. A. (2012). Landslide susceptibility mapping (LSM) at Kota Kinabalu, Sabah, Malaysia using factor analysis model (FAM). Journal of Advanced Science and Engineering Research, 2(1), 80-103.

[11] Sharir, K., Roslee, R., Ern, L. K., & Simon, N. (2017). Landslide Factors and susceptibility mapping on natural and artificial slopes in Kundasang, Sabah. Sains Malaysiana, 46(9), 1531–1540. doi:10.17576/jsm-2017-4609-23.

[12] Krishnan, R. B., Sharir, K., Baba, M. F., Mok, B., Warnana, D. D., Lestari, W., Dambul, R., Wen, W. Z., Ismail, A., & Roslee, R. (2025). Landslide Susceptibility Mapping Using Weights of Evidence Model: A Case Study from Pekan Nabalu to Kundasang, Sabah, Malaysia. International Journal of Design & Nature and Ecodynamics, 20(05), 1029–1036. doi:10.18280/ijdne.200508.

[13] Mohd Salleh, M. R., Norhairi, N. H. A., Ismail, Z., Abd Rahman, M. Z., Abdul Khanan, M. F., Asmadi, M. A., Razak, K. A., Tam, T. H., & Osman, M. J. (2022). Classification of Translational Landslide Activity using Vegetation Anomalies Indicator (Vai) in Kundasang, Sabah. The International Archives of the Photogrammetry, Remote Sensing and Spatial Information Sciences, XLVI-4/W3-2021, 247–256. doi:10.5194/isprs-archives-xlvi-4-w3-2021-247-2022.

[14] Roslee, R., Tahir, S., & Laming, A. (2005). Engineering Geological Investigation on Slope Failure along Bundu Tuhan to Kundasang Road, Sabah, Malaysia. Warta Geologi (Newsletter of the Geological Society of Malaysia), Geological Society of Malaysia (GSM), Kuala Lumpur, Malaysia.

[15] Dos, J. P., Roslee, R., Sharir, K., & Warnana, D. D. (2024). Quantitative Landslide Hazard Assessment Using Frequency Ratio Model: A Case Study from SMK Kundasang, Sabah, Malaysia. International Journal of Design and Nature and Ecodynamics, 19(3), 1007–1018. doi:10.18280/ijdne.190330.

[16] Roslee, R., Pirah, J. A., Madri, A. N., & Zikiri, M. F. (2020). Applicability of the Geological Strength Index (GSI) Classification for the Trusmadi Formation at Sabah, Malaysia. Earth Science Malaysia, 4(1), 77–81. doi:10.26480/esmy.01.2020.77.81.

[17] Jabatan Kerja Raya (JKR) Sabah. (2001). Report on Geotechnical Investigation and Conceptual Design of The Slope Remedial Works at KM93.3, Jalan Tamparuli – Ranau, Sabah. Jabatan Kerja Raya (JKR) Sabah, Kota Kinabalu, Malaysia.

[18] Rosli, M. I., Mohd Kamal, N. A., & Razak, K. A. (2021). Assessing Earthquake-induced Debris Flow Risk in the first UNESCO World Heritage in Malaysia. Remote Sensing Applications: Society and Environment, 23, 100550. doi:10.1016/j.rsase.2021.100550.

[19] IKRAM Sabah. (2000). Geotechnical Investigation Report into the Failure and Earth Movement at SMK Kundasang, Ranau, Sabah. IKRAM Sabah, Kota Kinabalu, Malaysia.

[20] Jabatan Kerja Raya (JKR) Sabah. (2001). Report on Geotechnical Investigation and Conceptual Design of The Slope Remedial Works at KM94.1, Jalan Tamparuli – Ranau, Sabah. Jabatan Kerja Raya (JKR) Sabah, Kota Kinabalu, Malaysia.

[21] Cressie, N. (1990). The origins of kriging. Mathematical Geology, 22(3), 239–252. doi:10.1007/BF00889887.

[22] Cressie, N. A. C. (1993). Statistics for Spatial Data. Wiley Series in Probability and Statistics, John Wiley & Sons, Hoboken, United States. doi:10.1002/9781119115151.

[23] Minnitt, R., Assibey-Bonsu, W., & Camisani-Calzolari, F. (2003). Keynote address: A tribute to Prof. DG Krige for his contributions over a period of more than half a century. Operations Research, 405-408.

[24] Pawlowsky-Glahn, V., & Olea, R. A. (2004). Geostatistical Analysis of Compositional Data. In Geostatistical Analysis of Compositional Data. Oxford University Press. doi:10.1093/oso/9780195171662.001.0001.

[25] Boumpoulis, V., Michalopoulou, M., & Depountis, N. (2023). Comparison between different spatial interpolation methods for the development of sediment distribution maps in coastal areas. Earth Science Informatics, 16(3), 2069–2087. doi:10.1007/s12145-023-01017-4.

[26] Ho, V. H., Morita, H., Ho, T. H., Bachofer, F., & Nguyen, T. T. (2025). Comparison of geostatistics, machine learning algorithms, and their hybrid approaches for modeling soil organic carbon density in tropical forests. Journal of Soils and Sediments, 25(5), 1554–1577. doi:10.1007/s11368-025-04027-5.

[27] Zarychta, R., & Zarychta, A. (2025). Application of geostatistical approach in generating DEM for relief studies using UAV in forest areas. Geomorphology, 487, 109916. doi:10.1016/j.geomorph.2025.109916.

[28] Zhakypbek, Y., Rysbekov, K., Lozynskyi, V., Mikhalovsky, S., Salmurzauly, R., Begimzhanova, Y., Kezembayeva, G., Yelikbayev, B., & Sankabayeva, A. (2025). Geospatial and Correlation Analysis of Heavy Metal Distribution on the Territory of Integrated Steel and Mining Company Qarmet JSC. Sustainability (Switzerland), 17(15), 7148. doi:10.3390/su17157148.

[29] Banerjee, S., Carlin, B. P., & Gelfand, A. E. (2014). Hierarchical Modeling and Analysis for Spatial Data. Chapman and Hall/CRC, New York, United States. doi:10.1201/b17115.

[30] Kokkala, A., & Marinos, V. (2022). An engineering geological database for managing, planning and protecting intelligent cities: The case of Thessaloniki city in Northern Greece. Engineering Geology, 301, 106617. doi:10.1016/j.enggeo.2022.106617.

[31] Chilès, J., & Delfiner, P. (2012). Geostatistics. Wiley Series in Probability and Statistics. John Wiley & Sons, Hoboken, United States. doi:10.1002/9781118136188.

[32] Qu, L., Lu, H., Tian, Z., Schoorl, J. M., Huang, B., Liang, Y., Qiu, D., & Liang, Y. (2024). Spatial prediction of soil sand content at various sampling density based on geostatistical and machine learning algorithms in plain areas. CATENA, 234, 107572. doi:10.1016/j.catena.2023.107572.

[33] Oliver, M. A., & Webster, R. (1990). Kriging: A method of interpolation for geographical information systems. International Journal of Geographical Information Systems, 4(3), 313–332. doi:10.1080/02693799008941549.

[34] Isaaks, E. (2005). The Kriging Oxymoron: A Conditionally Unbiased and Accurate Predictor (2nd Edition). In: Leuangthong, O., Deutsch, C.V. (eds) Geostatistics Banff 2004. Quantitative Geology and Geostatistics, 14. Springer, Dordrecht, Netherlands. doi:10.1007/978-1-4020-3610-1_37.

[35] Esri. (2014). ArcGIS Desktop (10.3). Esri, Kranzberg, Germany. Available online: http://www.esri.com/software/arcgis (accessed on December 2025).

[36] Nwaila, G., Tolmay, L., & Burnett, M. (2024). Geostatistics Notes for Practitioners. CRC Press, Boca Raton, United States. doi:10.1201/9781032650388.

[37] Webster, R., & Oliver, M. A. (2007). Geostatistics for Environmental Scientists. John Wiley & Sons, Hoboken, United States. doi:10.1002/9780470517277.

[38] Liu, Y., Tian, G., Wang, S., Satyanaga, A., & Zhai, Q. (2022). Parametric Analysis of Rainfall-Induced Loess Soil Slope Due to the Rainwater Infiltration. Urban Science, 6(3), 54. doi:10.3390/urbansci6030054.

[39] BS 5930:2015. (2015). Code of practice for ground investigations (+A1:2020). British Standard International (BSI), London, United Kingdom.

[40] Baum, R. L., & Godt, J. W. (2010). Early warning of rainfall-induced shallow landslides and debris flows in the USA. Landslides, 7(3), 259–272. doi:10.1007/s10346-009-0177-0.

[41] Tetteh, F. K., Abbey, S. J., Booth, C. A., & Nukah, P. D. (2025). Current understanding and uncertainties associated with climate change and the impact on slope stability: A systematic literature review. Natural Hazards Research, 5(3), 563–595. doi:10.1016/j.nhres.2025.01.011.

[42] Roslee, R., & Krishnan, R. B. (2023). Landslide susceptibility assessment in Sabah, Malaysia: A bivariate frequency ratio approach. Science, Engineering and Health Studies, 17. doi:10.69598/sehs.17.23020004.

[43] Goovaerts, P. (1997). Geostatistics for Natural Resources Evaluation. Oxford University Press, Oxford, United Kingdom. doi:10.1093/oso/9780195115383.001.0001.

[44] Sun, L., Zhou, J. L., Cai, Q., Liu, S., & Xiao, J. (2021). Comparing surface erosion processes in four soils from the Loess Plateau under extreme rainfall events. International Soil and Water Conservation Research, 9(4), 520–531. doi:10.1016/j.iswcr.2021.06.008.

[45] Szabó, J. A., Keller, B., Centeri, C., Hatvani, I. G., Kovács, J., Szalai, Z., & Jakab, G. (2023). Varying particle size selectivity of soil erosion along a cultivated catena. Open Geosciences, 15(1), 20220585. doi:10.1515/geo-2022-0585.

[46] Zhu, F., Li, Y., & Cheng, J. (2021). Size characteristics of sediments eroded under different Masson pine litter covers in south China. Water (Switzerland), 13(16), 2190. doi:10.3390/w13162190.